A Series Resonant Converter-Based Multichannel LED Driver With Inherent Current Balancing and Dimming Capability

Taha Nurettin Gücin, Bekir Fincan, and Muhammet Biberoğlu

***Abstract*—This study proposes a high-efficiency light-emitting-diode (LED) driver based on the series resonant converter (SRC) topology. As the major requirement from LED driver circuits is the ability of providing constant current for maintaining a certain luminescence level, it is utilized that the SRC operates as a frequency-controlled constant current source when the switching frequency is lower than half of the resonance frequency. This approach ensures a reliable and dimmable constant current power supply that can operate in an open-loop configuration. A design procedure for the proposed multichannel LED driver is given and experimental results for a prototype that is capable of delivering 50 V–0.35 A output for six channels are presented. It is also shown that the proposed driver is capable of ensuring high efficiency values (92%–93.5%) for a wide output power (14–58 W).**

***Index Terms*—Light-emitting-diode (LED), LED driver, resonant converters, series resonant converter (SRC).**

I. Introduction

THE light-emitting-diode (LED) technology has been the main focus point in lightning applications due to their advantageous properties such as being shock resistant, durable, and having longer operation life. Moreover, they are five times more efficient compared to incandescent lighting solutions [1], [2]. Thus, they are utilized in a wide range of applications, such as traffic and street lightning, indoor lightning, automotive applications, etc. Although they have distinct advantages, LEDs suffer from being temperature sensitive. Furthermore, due to the production process, their parameters are very erratic; even LEDs from same packaging usually exhibit different parameters. Therefore, LEDs usually require special reliable drivers that are able to supply current with a constant value, in order to ensure a certain luminescence level [1], [2].

The increasing demand for LED technology resulted in numerous studies proposing various driver circuits. This section is aimed to provide an extensive review on LED drivers,

Manuscript received January 16, 2018; revised April 9, 2018; accepted May 14, 2018. Date of publication May 17, 2018; date of current version February 5, 2019. Recommended for publication by Associate Editor J. M. Alonso. *(Corresponding author: Taha Nurettin Gücin.)*

T. N. Gücin and B. Fincan are with the Electrical Engineering Department, Istanbul Technical University, Istanbul 34172, Turkey (e-mail:

where a constant voltage value is ensured. The switching device of boost stage is comprised of N number of MOSFETs connected in series, instead of a single one. Each LED string is connected in parallel with one MOSFET. In this structure, it is aimed to power up each string once in a switching cycle sequentially. For powering the nth string, the associated nth MOSFET is turned OFF, while all other MOSFETs are turned ON. The sequencing logic is similar to one presented in [5]. Thus, again an FPGA is employed for implementing the sequencer logic.

An approach similar to [5] is presented in [7]. In contrast to [5], the boost converter operates in dc–dc converter mode instead of the PFC mode. Furthermore, the way how LED strings are connected to boost converter is different. However, the basic principle for enabling current balancing is again the sequencing logic mentioned earlier.

The study [8] presents a multichannel LED driver based on multioutput flyback converter. The operation principle is based on capacitor charge balancing, which is extended to multioutput applications. Each LED string is connected to a separate secondary winding of a flyback transformer, while each LED string is connected to each other through a current balancing capacitor. The current in one LED string is sensed and used for controlling the MOSFET of the flyback converter.

In [9], a different approach to multioutput LED drivers is presented. A conventional flyback converter with two secondary winding is used for supplying multiple dc voltage outputs. One winding is used for producing a "master source," while the second output is used for generating other multiple "slave sources." The current regulation is achieved by magnetic-amplifier (mag-amp) postregulators, which are based on magnetic saturation principle. While a feedback controller for flyback converter for obtaining a constant dc voltage is required, each mag-amp regulator also needs separate controllers to balance their currents. The study also demonstrates an implementation of PWM dimming and phase-shift (PSPSM) dimming schemes.

A single-inductor multiple-current output (SIMCO) buck converter for multichannel LED driver applications is presented in [10]. The buck converter is operated at CCM. The LED string with the highest voltage has the least current, while the currents flowing through the others depend on the voltage differences. Thus, each string, except the one with highest voltage, has a series connected MOSFET, which is switched ON and OFF for creating N number of constant-current outputs. Basically, the MOSFET of the buck converter is controlled in average current mode control so that it supplies the desired current flowing through the LED string with the highest voltage. The currents in other strings are dimmed using the associated MOSFETs. The proposed scheme requires each LED string current to be sensed and controlled separately. The studies reviewed in this chapter are summarized in Table I.

A single-stage multiple-output LED driver derived from buck converter is presented in [11] and [12]. The PFC and bus regulation is achieved by the buck converter, which is shared by all LED strings. The current regulation in each string is achieved by a MOSFET employed in each string. This study also incorporates the time-multiplexing (TM) control scheme, which ensures only one string to be included in the closed loop at any given time.

This study [13] proposes another boost converter based SIMO parallel-LED driver operated with a TM control scheme. The TM control loop powers only one string during one switching cycle, while other strings are turned OFF. In this study, the switch and the inductor of the boost converter is shared with each LED string, while it is operated in discontinuous conduction mode (DCM) to prevent cross-regulation. Each string is employed with an active rectifier circuit (AR) and a MOSFET, so that they would enable the regulation of each bus voltage and connection of the string to the current sensing resistor, respectively.

Finally, the study [14] discusses the scalability of a buck converter based single-inductor dual-output LED driver, where a digital quasi-hysteretic finite-state machine control scheme is utilized. This control scheme allows eliminating the loop compensation, so that the closed-loop controller is simplified. The constraints for maximum allowable number of strings are discussed in detail.

B. Review of Multichannel LED Drivers Utilizing Resonant Converters

Since this study proposes a resonant converter based LED driver, it is intended to demonstrate how resonant converters are utilized in LED driver applications. Consequently, the difference of the proposed approach can be easily perceived.

In [15], an LED driver consisting of an *LCLC* series–parallel resonant inverter and *LCL*-T resonant rectifiers is proposed. The study utilizes the fact that *LCL*-T resonant rectifiers are inherently capable of supplying constant current output, while an constant input ac voltage is supplied by the resonant inverter. Thus, while the voltage output of the resonant inverter is regulated with feedback controller, current balancing is inherently enabled by *LCL*-T circuits employed for each LED string [15].

In study [16], a high-frequency ac–ac resonant converter was developed by integrating a DCM boost converter and an *LCLC* series–parallel resonant converter in a single stage. It is aimed to achieve PFC and a high-frequency sinusoidal ac link. The developed ac–ac converter is then used to improve the LED driver presented in [15] by employing the PFC ability. Although the integrated PFC and ac link stage requires feedback controllers, the *LCL*-T circuits inherently supply constant current output. However, the amount of utilized circuit elements in the proposed scheme are relatively high [16].

The study [17] offers a two-stage MC^3 LED driver that is comprised of a buck converter and CLL resonant converter. In the proposed configuration, it is aimed to regulate the output of the buck converter through a feedback loop from one of the LED strings, while the CLL resonant converter is constantly operated at series resonant frequency. The current balancing is ensured by transformers that are connected in series at the output of the resonant tank. However, each output requires one transformer. Since a voltage doubler structure is utilized at the rectification stage of the resonant circuit, one transformer can drive two LED strings. Dimming can be achieved by regulation of the buck converter output [17].

In [18], a capacitor-isolated LED driver with inherent current balancing is proposed. The architecture is based on the

TABLE I
REVIEW OF MULTICHANNEL LED DRIVER CIRCUITS

		[3]	[4]	[5]	[6]	[7]	[8]	[9]	[10]	[11], [12]	[13]	[14]
PFC		X	X	+	+	X	X	X	X	+	X	X
cosφ		X	X	0.99	0.92-0.96	X	X	X	X	0.99	X	X
Component for PFC		X	X	Boost	Boost	X	X	X	X	Buck	X	X
Component for DC Bus Regulation		SEPIC	Boost	SIMO Buck		SIMO Boost	Multi-Out. Flyback	Forward	SIMCO Buck		SIMO Boost	SIMO Buck
Component for Current Balancing		Error Amp.	MOSFET	Sequenced MOSFETs	Sequenced MOSFETs	Sequenced MOSFETs	Capacitors	Mag-Amps	MOSFETs	MOSFETs		
Dimming Ability		PWM	PWM	PWM	PWM	N/A	N/A	PWM or PSPWM	PWM	PWM	+	+
Feedback Required for	PFC	X	X	+	+	X	X	X	X	+	X	X
	DC Bus Regulation	+	+	+	-	+	+	+	+		+	+
	Current Balancing	+	+	-	-	-	-	+	+	+		
Number of Required Components for N LED Strings	Diode	N+1	2	N+5	N+4	N	N	N+2	N+1	N+5	0	0
	MOSFET	N+1	N+2	N+2	N	N+1	N+1	2	N	N+1	1+2N*	2+N
	Transformer	0	0	0	0	0	0	1 with 2 Outputs	0	0	0	0
	Inductor	2	1	2	1	1	1	3	1	1	1	1
	Capacitor	2	1	N+1	N	N	2N	3	N	N	2N	N
Power, W		35	N/A	4.6	N/A	12.4	20	16.5	12	9 - 30	N/A	~ 1
Efficiency, %		85-88	50-90	76.6	50-90	93	78.5-83.5	86-88	91	82 - 89	N/A	N/A
Current Balancing Error, %		N/A	N/A	0.38-1.93	N/A	0.12-2	1	N/A	N/A	N/A	1.7	N/A

X: Study does not investigate this aspect, **N/A:** No certain data available, **+:** Positive, **-:** Negative
***:** Also requires 6.N transistors for active rectifier circuitry.

series resonant converter (SRC), where the resonant capacitor also provides isolation with two-output rectifier topology that drives two LED strings. Thus, the circuit is more efficient and compact compared to the transformer isolated converters. In the proposed driver, a series resonant tank for each of the two LED strings is employed. The current balancing for each resonant tank is achieved by coupled inductors employed in series with resonant elements. Conventional frequency control is utilized for controlling the output currents [18].

Another multichannel LED driver based on the SRC is proposed in [19]. It includes a hybrid passive current balancing method, which is very similar to the study presented in [18]. The only difference is that the voltage doubler configuration is adopted at the output of the SRC [19].

In [20], a multioutput LED driver based on *LLCC* resonant converter is proposed. In the proposed scheme, each LED string requires a separate output winding from the transformer. The total output current is sensed for forming a feedback loop that is used for frequency modulation of the resonant converter. Secondary side resonant capacitors of the resonant circuit enable passive current balancing among LED strings [20].

The multichannel LED driver in [21] includes a quasi-two-stage converter. In this structure, an *LLC* resonant converter is utilized for bus voltage regulation for the LED strings. Each output module of the converter has two outputs so that it drives two LED strings. The current balancing between two LED strings, which are connected to the same output module, is achieved by capacitors. On the other hand, nonisolated buck-boost converters employed at each output module ensure current balance between other output modules. In this driver circuit, *LLC* resonant converter and all buck-boost type current regulators require feedback controllers [21].

The study [22] developed *CLC*-T resonant circuits, which are able to supply constant current output given that a sinusoidal input voltage with constant magnitude is ensured. A full-bridge inverter is utilized for generating ac input voltages. For eliminating harmonics, an additional inductor is also employed at inverter output, resulting in an *LCLC* series–parallel resonant inverter. The inverter is operated at fixed-frequency under duty-cycle control. An application of the PWM dimming scheme is also demonstrated [22].

The study [23] utilized a soft-switched ac–dc converter, which is developed by integrating the totem-pole bridgeless PFC boost converter and half-bridge *LLC* resonant converter. The circuit also enables an increased bus voltage ripple so that the need for electrolytic capacitors can be avoided. Twin-bus buck type current regulators are used for current balancing at the output of the *LLC* resonant converter. These current regulators are also utilized for PWM dimming. The ac–dc converter and each current regulator require feedback controllers. The complexity of the circuitry is relatively high [23].

In [24], another multichannel LED driver is offered. The study incorporates an *LLC* resonant converter for ensuring a constant voltage output. The current regulation among each LED string is achieved by several passive elements such as diodes and capacitors. Moreover, each LED string requires a separate output winding of transformer for achieving current balance. The study demonstrates the ability of PWM dimming for controlling the total current amount by a single MOSFET [24].

Finally, in [25], an LED driver, which is very similar to the one presented in [24], is demonstrated. In addition to [24], an initial current regulator is also employed in the investigated LED driver. The studies included in this chapter are summarized in Table II.

C. Conclusion on Literature Survey

As it is reviewed above, there are lots of proposed approaches to multichannel LED driver solutions that have been very popular recently. All of the reviewed studies involve at least one closed-loop controller for regulating the output current. The requirement for controllers generally tend to increase with the advancing circuit complexity. However, circuit complexity and accompanying costs are usually the major obstacles for the commercialization of such relatively new technologies.

TABLE II
REVIEW OF MULTICHANNEL LED DRIVER CIRCUITS UTILIZING RESONANT CONVERTERS

		[15]	[16]	[17]	[18]	[19]	[20]	[21]	[22]	[23]	[24]	[25]	Proposed
PFC		X	+	X	X	X	X	X	X	+	X	X	X
cosφ		X	0.95	X	X	X	X	X	X	0.99	X	X	X
Component for PFC		X		X	X	X	X	X	X		X	X	X
Component for DC/AC Bus Regulation		LCLC Res. Inv.	Integ. Boost + LCLC Inverter	Buck + CLL Res. Conv.	SRC	SRC	LLCC Res. Conv.	LLC Res. Conv.	LCLC Res. Conv.	Boost + LLC Res Conv.	LLC Res. Conv.	LLC Res. Conv.	SRC
Component for Current Balancing		LCL-T Rect.	LCL-T Rect.	Transf.	Coupled Ind. and Cap.	Coupled Ind. and Cap.	Cap.	Cap. and Buck-Boost Conv.	CLC-T Circuits	Twin-Bus Buck Type Current Conv.	Cap.	Cap.	
Dimming Ability		+	-	+	+	-	+	N/A	PWM	+	PWM	PWM	Inherent
Feedback Required for	PFC	X	+	X	X	X	X	X	X	+	X	X	X
	DC/AC Bus Regulation	+		+	+	+	+	+	+	+	+	+	-
	Current Balancing	-	-	-	-	-	-	+	-	+	-	-	-
Number of Required Components for N LED Strings	Diode	4N	4N+4	N+1	2N	N	4N	5N/2	N+4M**	N+7	3N	3N	N
	MOSFET	4	2	3	2	2	2	N/2+2	N+M+4**	N+2	2	3	2
	Transformer	1	1	N/2	0	1	1 with N Outputs	1 with N/2 Outputs	1	1	1 with N Outputs	1 with N Outputs	0
	Inductor	2N+2	2N+4	3	N+1 CM	N/2+1	2	N+1	2	1	1	1	N/2
	Capacitor	2N+2	2N+6	N	2N	N/2+2	2N+2	3N/2 +1	3N/2+ 2M+1**	N+5	3N/2 +1	3N/2 +1	3N/2+2
Power, W		200	130	27	60	80	150	120	20	100	140	N/A	14 - 58
Efficiency, %		>92	90	93-95	91-94	N/A	86-96.5	95	91	86-94	95	86	92 - 93.5
Current Balancing Error, %		<1	N/A	<3	2-4.5	N/A	N/A	N/A	N/A	N/A	N/A	1.7	0.5 - 2

X: Study does not investigate this aspect, **N/A:** No certain data available, **+:** Positive, **-:** Negative
****:** For study [22], N is used for LED strings that are connected to half-wave rectifiers, while M denotes the number of LEDs connected to full-wave rectifiers.

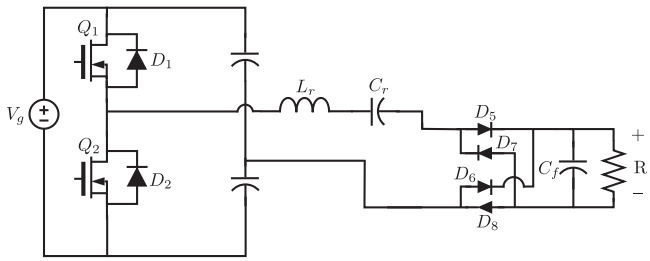

Fig. 1. Illustration of half-bridge SRC.

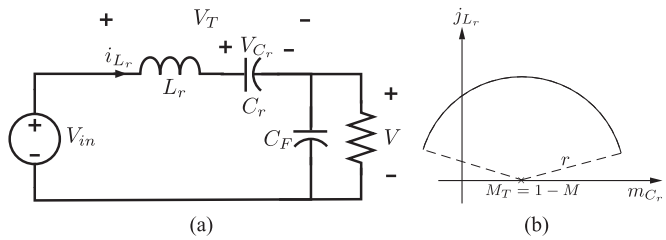

Fig. 2. (a) Half-bridge SRC reduced to an equivalent circuit. (b) Normalized state plane trajectory for the circuit of Fig. 2(a).

Due to the reasons mentioned above, this study aims to offer a simple but effective solution for multichannel LED applications by making use of the fact that the SRC operates as a constant current source (CCS) at half resonance frequency. Furthermore, despite some limitations, it also enables dimming when operated below half resonance frequency. Consequently, the costs and space requirements of the LED driver can be reduced by the simplicity of the offered driver circuit.

It is also worth mentioning that this study assumes that the proposed LED driver is connected to a regulated dc bus, which may be the output of a PFC converter or a regulated dc bus.

II. STATE PLANE ANALYSIS (SPA) OF THE SRC

In this study, the exact solutions of the SRC using SPA is briefly summarized so that the operation principles of the proposed circuit can be understood. The details for SPA of the SRC can be found in [26]. The half-bridge SRC is illustrated in Fig. 1.

Assuming that the input voltage of the resonant tank is in a square-wave form with the magnitudes $V_{\text{in}} = V_g/2$, $V_{\text{in}} = -V_g/2$ and a constant load voltage V is assured with the well-designed output filter configuration, the SRC can be reduced to an equivalent circuit. Then, the analysis of the SRC can be performed using this equivalent circuit in Fig. 2(a).

The term V_T is called terminal voltage, which is $V_T = V_{\text{in}} - V$. The circuit can be expressed using the following differential equations:

$$L\frac{di_{L_r}(t)}{d(t)} = V_T - v_C(t) \tag{1}$$

$$C\frac{dv_{C_r}(t)}{d(t)} = i_{L_r}(t). \tag{2}$$

Often, the SPA results in more simplified equations, when a normalization procedure is performed and the equations become unitless. For this purpose, all variables in the equations are divided by some predetermined "base values" to obtain unitless quantities. Thus, using some base values for voltage, resistance and current variables, as given in Table III, a normalization procedure is performed. The state equations in normalized form become

$$\frac{1}{\omega_0}\frac{dj_{L_r}(t)}{d(t)} = M_T - m_{C_r}(t) \tag{3}$$

$$\frac{1}{\omega_0}\frac{dm_{C_r}(t)}{d(t)} = j_{L_r}(t). \tag{4}$$

TABLE III
BASE VALUES AND NORMALIZED PARAMETERS

Base Values	
Base Impedance [Ω]	$R_{base} = \sqrt{L_r/C_r}$
Base Voltage [V]	$V_g/2$
Base Current [A]	$V_{base}/R_{base} = V_g/2.R_{base}$
Base Power [W]	$P_{base} = V_g^2/4.R_{base}$
Base Frequency [Hz]	$f_{base} = 1/2.\pi.\sqrt{L_r.C_r}$
Normalized Parameters	
Normalized Load Voltage	$M = V/V_{base}$
Normalized Load Current	$J = I/I_{base}$
Normalized Capacitor Voltage	$m_{C_r}(t) = v_{C_r}/V_{base}$
Normalized Inductor Current	$j_{L_r}(t) = i_{L_r}/I_{base}$
Tank Resonance Angular Frequency	$w_0 = 1/\sqrt{L_r.C_r} = w_{base}$
Tank Resonance Frequency	$f_0 = w_0/2\pi$
Normalized Switching Frequency	$F = f_s/f_0$
Angular Length of Half Switching Period	$\gamma = \pi/F$
Diode Conduction Angle	$\alpha = \omega_0 t_\alpha$
Transistor Conduction Angle	$\beta = \omega_0 t_\beta$

The solutions of these differential equations are

$$m_{C_r}(t) = M_T + A.\cos(\omega_0 t - \varphi) \tag{5}$$

$$j_{L_r}(t) = -A.\sin(\omega_0 t - \varphi). \tag{6}$$

When interpreted in detail, one can see that these equations represent a circle centered at the point ($m_{C_r} = M_T$, $j_{L_r} = 0$). The radius of the circle, r, is dependent on the initial conditions. This solution is illustrated in Fig. 2(b).

Since a general solution for the equivalent circuit is achieved, this solution can be applied for all the operation subintervals of the SRC, so that a complete state plane trajectory may be obtained. While CCM operation has four operational subintervals, Subintervals 1–4, another additional subinterval, Subinterval 5, occurs when it is operated in DCM. This paper aims to operate the SRC in k = 2 DCM mode, where k is the number of complete half-cycle ringing during half of the switching period. The operational subintervals observed during k = 2 DCM operation are as follows:

1) *Subinterval 1:* The first subinterval of CCM is attained when the terminal voltage is $V_T = +\frac{V_g}{2} - V$. In this mode Q1, D5, D8 conduct.

2) *Subinterval 2:* The second subinterval occurs when the terminal voltage is $V_T = +\frac{V_g}{2} + V$. In this mode D1, D6, D7 conduct.

3) *Subinterval 3:* The third subinterval of CCM is attained when the terminal voltage is $V_T = -\frac{V_g}{2} + V$. In this mode Q2, D6, D7 conduct.

4) *Subinterval 4:* The fourth subinterval occurs when the terminal voltage is $V_T = -\frac{V_g}{2} - V$. In this mode D2, D5, D8 conduct.

5) *Subinterval 5: (Additional DCM Subinterval X)* It is sometimes possible for all output diodes of the SRC to be reverse-biased. In this case, the current in the resonant tank is equal to zero and the value of the resonant capacitor remains same during this interval, denoted by "Subinterval X."

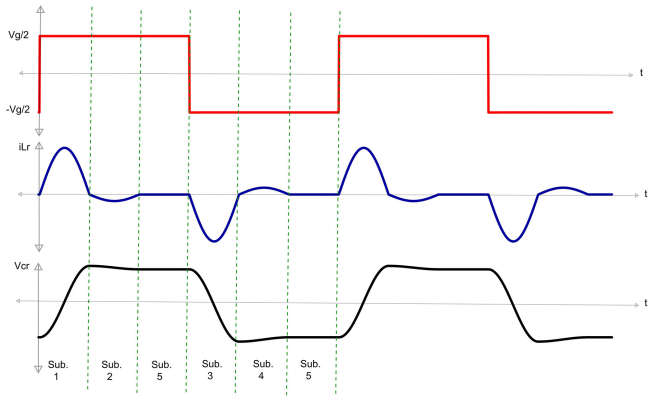

Fig. 3. Operation waveforms of the SRC and for k = 2 DCM operation.

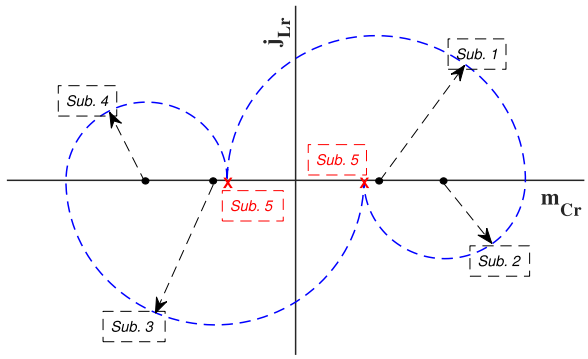

Fig. 4. Complete state plane trajectory for k = 2 DCM operation.

The operational waveforms and complete state plane trajectory of the k = 2 DCM are illustrated in Figs. 3 and 4, respectively.

Since the operation modes of the SRC are now analyzed and visualized as state plane trajectories, the problem of solving differential equations numerically has been reduced to a geometrical problem that can be solved for these trajectories. Using basic geometrical principles and trigonometric identities, the solutions for M, J, and J_{crit}, normalized critical output current value for DCM boundary condition, can be derived. The output equation for the k = 1 CCM case is

$$M^2.\sin^2\left(\frac{\gamma}{2}\right) + \left(\frac{J.\gamma}{2} - 1\right)^2.\cos^2(\gamma/2) = 1. \tag{7}$$

The output characteristics of the SRC in k = 1 CCM are illustrated in Fig. 5(a). These output characteristics describe the relationship between J and M for different values of F. As it is seen in Fig. 5(a), the SRC operates as a CCS at $F = 0.5$ for normalized output voltage values of $0 < 1 < M$.

On the other hand, the "k = 2 DCM" mode, where the resonant tank current rings for two half-cycles (k = 2) during a half switching period, results in the following normalized output voltage and current equations

$$M = \frac{4FR}{\pi R_{\text{base}}} = \frac{4F}{\pi Q} \tag{8}$$

$$J = \frac{4F}{\pi}. \tag{9}$$

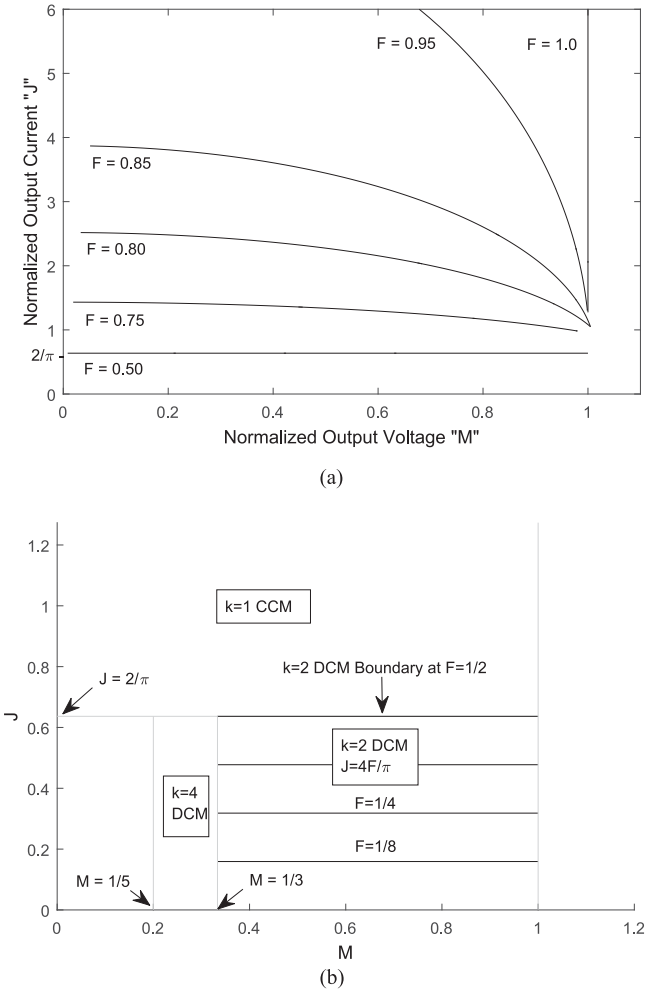

Fig. 5. Exact output characteristics of the SRC (a) in CCM and (b) in k = 2 DCM.

Here Q is defined as $Q = R_{\text{base}}/R$. The boundaries of this mode are given by

$$1 > M > \frac{1}{3} \tag{10}$$

$$\frac{2}{\pi} > J > 0 \tag{11}$$

$$\frac{1}{2} > F > 0. \tag{12}$$

The output characteristics of this mode are graphically illustrated in Fig. 5(b).

III. Utilizing the SRC for LED Driver Applications

A. Basic Principle of the Proposed Approach

As it can be seen from the output characteristics, given in Fig. 5, the SRC operates as a CCS on the CCM–DCM boundary when the switching frequency is equal to half resonance frequency, $f_s = f_0/2$. Considering the fact that LEDs require a constant current supply for a certain illumination level, it can be seen that the SRC offers a simple solution. The required output current for the LEDs can be obtained by the correct design.

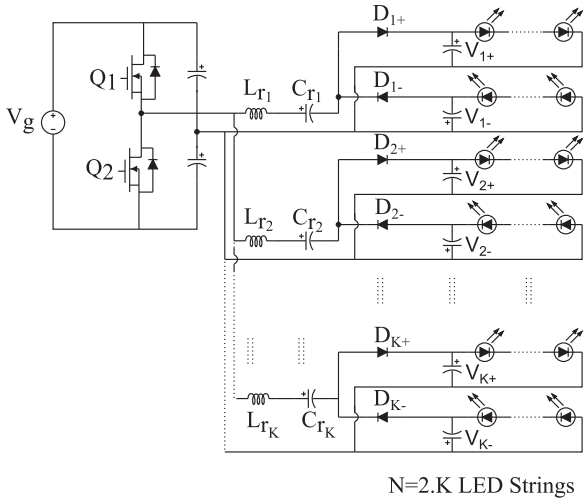

Fig. 6. Proposed configuration of SRC for LED drive application.

Moreover, the output characteristics illustrated in Fig. 5(b) exhibit that the constant output current of the SRC operating in "k = 2 DCM" is linearly dependent on the switching frequency. Thus, the output current of an LED driver based on SRC can be regulated by simply adjusting the switching frequency, which inherently enables dimming property. However, it should be noted that the normalized output voltage is bounded by the condition, $1/3 < M < 1$. This is a limitation of the proposed driver circuit, which determines the maximum and minimum number of LEDs that can be connected in series for a single string.

B. Derivation of the SRC-Based Multichannel LED Driver

The SRC illustrated in Fig. 1 can drive a single LED string with constant current. The number of series connected LEDs in one string can be varied, considering the boundary given in (10). When typical LED driver power levels are considered, it is determined to utilize a half-bridge inverter topology for generating an ac bus link, so that the number of required components are reduced.

For deriving a multichannel LED driver, it is intended to utilize separate resonant tanks for each LED string. Each resonant tank is connected to the same half-bridge inverter so that a multichannel LED driver is achieved.

The number of components can be further reduced by employing half-wave rectifier configuration at the output, as shown in Fig. 6, instead of the full-wave rectification scheme shown in Fig. 1. Furthermore, the losses caused by rectifier diodes are reduced due to decreased number of diodes per LED string. However, in the case of half-wave rectifier configuration the followings must be taken into account.

1) A single half-wave rectifier draws energy from the resonant tank during only one half of the switching period. If no energy is extracted from the remaining half period, the operation of the SRC may be influenced. Thus, if half-

wave rectifier topology is employed, each output module must have two half-wave rectifiers operating at compliment halves of a single switching period. In this study, two LED strings connected at one output module are referred as "LED String Couples." Consequently, the total string number, N, is always an even number, $N = 2K$. Obviously, K is the number of "LED String Couples."

2) The full-wave rectification case requires a separate resonant tank and four diodes for each string. On the other hand, the half-wave rectification case require one resonant tank and two diodes for two LED Strings. Thus, the number of required components are decreased.
3) Since the half-wave rectifier draws current only during half period, the value of the average output current is only half of the full-wave rectifier case. Thus, the resonant tank elements should be adjusted to obtain the same output current value as in the full-wave rectification case.

The proposed approach offers several distinct features that make the topology very suitable for multichannel LED driver applications. One of the major advantages is that a reliable constant current supply operating at open-loop configuration can be achieved, while the driver may incorporate different numbers of LEDs at each string. Moreover, the lack of the need for a closed-loop controller simplifies the design and reduces the costs and space requirements. Additionally, when compared to the reviewed studies, the driver circuitry is more simple and has less components, since the current balancing and dimming features are provided by inherent characteristics of the SRC at a single stage. Finally, the converter can operate at high efficiencies for a very wide output power range.

IV. Designing the Converter

For designing the SRC-based LED driver, the resonant tank elements must be determined. For this purpose, it is started by defining the normalized output current of the SRC, J

$$J = \frac{I}{I_{\text{base}}} = \frac{I}{V_{\text{base}}/R_{\text{base}}} = \frac{I.R_{\text{base}}}{V_{\text{base}}}. \tag{13}$$

One should pay attention to the fact that the base value for voltage was determined to be $V_{\text{base}} = V_g/2$, since a half-bridge SRC has been utilized for the proposed LED driver. If one decides to use a full-bridge SRC, the base value for voltage should be changed to $V_{\text{base}} = V_g$ so that the same normalized SPA equations can be used. Utilizing the base values, the above equation is expanded as follows:

$$J = \frac{2.I.R_{\text{base}}}{V_g}. \tag{14}$$

From Fig. 5, it can be observed that the maximum output current for "k = 2 DCM" operation is obtained at "k = 1 CCM" boundary, where the SRC is operated at half resonance frequency. The normalized output current at half resonance frequency is

$$J = \frac{2}{\pi}. \tag{15}$$

However, for the half-wave rectification case, the output current value is reduced to half, when compared to the full-wave rectification case. This is due to fact that the total electric charge is transferred from one resonant tank circuit to two LED strings. Thus, the normalized output current at half resonance frequency is now

$$J = \frac{1}{\pi}. \tag{16}$$

By equating (14) and (16), the value of base impedance can be calculated as

$$R_{\text{base}} = \sqrt{\frac{L_r}{C_r}} = \frac{V_{\text{base}}}{I.\pi} = \frac{V_g}{2.I.\pi}. \tag{17}$$

For better accuracy, the voltage drops due to diodes should be included in the design. These voltage drops can be considered as if they decrease the input voltage. Since this study employs a half-bridge SRC with half-wave rectification at the output, the effective input voltage can be considered as $V_{g,\text{effective}} = 2.(V_g/2 - V_{\text{drop}})$.

Equation (17) states the needed value of base impedance, R_{base}, for a required output current, I, at a certain input voltage, V_g. After determining the base impedance, a commercially available capacitor is chosen and the required inductance is calculated and winded. The required inductance and the resulting resonance frequency is then

$$L_r = C_r.R_{\text{base}}^2 \tag{18}$$

$$f_0 = \frac{1}{2.\pi.\sqrt{L_r.C_r}} = \frac{1}{2.\pi.\sqrt{R_{\text{base}}^2.C_r^2}} = \frac{1}{2.\pi.R_{\text{base}}.C_r}. \tag{19}$$

One limitation of the half-bridge SRC operated in "k = 2 DCM" is that the output voltage is bounded by the expression given in (10). Consequently, the upper and lower voltage limits of the driver can be expressed as

$$V_{\text{out,min}} < V_{\text{out}} < V_{\text{out,max}} \tag{20}$$

$$\frac{V_g}{6} < V_{\text{out}} < \frac{Vg}{2}. \tag{21}$$

Since the output voltage is restricted to a certain range, the minimum LED number n_{min} and maximum LED number $n_{\max}$ in one string are limited. Thus, these values can be calculated as

$$n_{\max} = \frac{V_{\text{out,max}}}{V_{f,\max}} = \frac{V_g}{2.V_{f,\max}} \tag{22}$$

$$n_{\text{min}} = \frac{V_{\text{out,min}}}{V_{f,\min}} = \frac{V_g}{6.V_{f,\min}} \tag{23}$$

where $V_{f,\max}$ is the forward voltage drop of a single LED at maximum forward current operation and $V_{f,\text{min}}$ is the forward voltage drop of a single LED at minimum/zero forward current operation. These values can be either found in datasheets provided by the manufacturer or they can be measured experimentally.

V. Experimental Results

In order to verify the proposed approach, it is decided to drive six LED strings, which employs blue LEDs by Edison Opto (2ES101BX00000001). The rated current of these LEDs

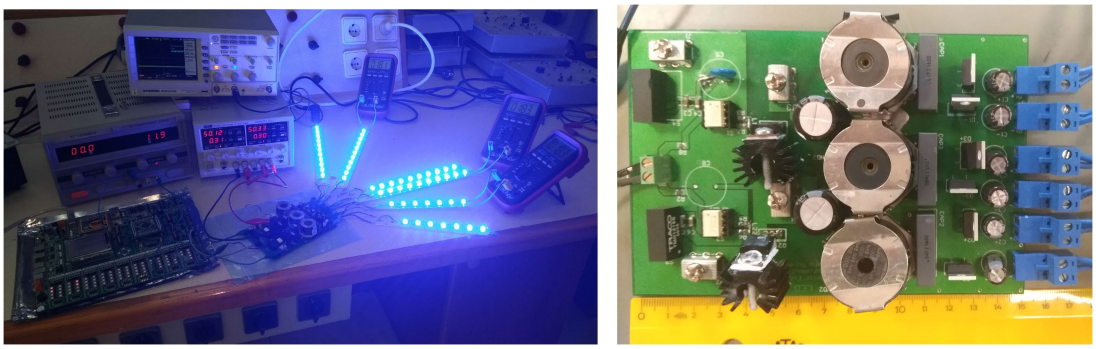

(a) (b)

Fig. 7. (a) Experimental setup and (b) implementation of the proposed LED driver.

TABLE IV
PREDETERMINED AND CALCULATED DESIGN PARAMETERS OF EXPERIMENTAL SETUPS

Design Calculations		
Parameter	Calculated Value	Realized Value
V_g (Predetermined)	100 V	
$V_{g,effective}$ (due to diode voltage drop)	98.3 V	
$I_{out,max}$	350 mA	351 mA
$V_{out,max}$ (from SPA) (Eq. 21)	49.15 V	
$V_{out,min}$ (from SPA) (Eq. 21)	16.38 V	
$V_{f,max}$	3.35 V	
$V_{f,min}$	2.95 V	
n_{max} (Eq. 22)	$14.92 \simeq 14$ rounding to nearest lower value for margin	
n_{min} (Eq. 23)	$5.65 \simeq 6$ rounding to nearest higher value for margin	
R_{base} (Eq. 17)	44.69	44.43
C_r (Chosen)	47 nF (chosen) 46.6 nF (measured)	
L_r (Eq. 18)	93.1 μH	92 μH
f_0 (Eq. 19)	76.406 kHz	76.866 kHz

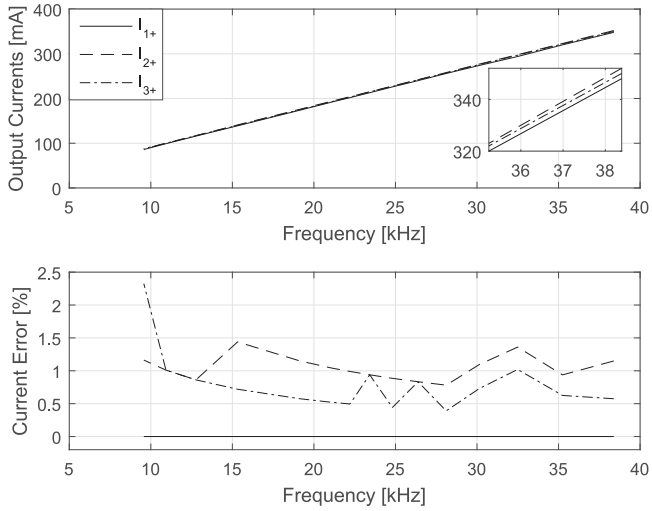

Fig. 8. Illustration of frequency-output current relationship and current balancing error.

are $I_f = 350$ mA. The forward voltage under $I_f = 350$ mA operation is $V_f = 3.35$ V, while it is $V_f = 2.95$ V for operation at $I_f = 100$ mA. The calculated design parameters are summarized in Table IV.

The experimental setup and the implementation of the proposed LED driver are shown in Figs. 7(a) and (b), respectively. The dimensions of the assembled circuit, which is capable of delivering 105 W in total, are $10.1 \times 15.1 \times 2.7$ cm. Thus, the power density of the prepared driver is 0.255 W/cm^3 = 4.18 W/in^3. Although most of the studies in the literature do not state the achieved power density, it can be easily seen that the power density achieved by the proposed driver is competitive with the studies presented in [12], [15], [17], and [23]. The power density of the circuit can be increased dramatically by increasing the switching frequency, of which SRC and resonant converters are capable of [26], [27]. Moreover, since the proposed driver is operated at k = 2 DCM, it benefits from zero current switching for the MOSFETs at the turn-OFF action. Additionally, during the turn-ON action of the MOSFETs, the current starts to increase from 0 A, which causes relatively less losses when compared to CCM operation. Consequently, it is possible to achieve frequencies around MHz range [26], [27] and higher power densities. Furthermore, the proposed driver requires less resonant tank inductance values for achieving higher output currents, as it can be referred from (17). Thus, designs for higher current output decreases the space needed for magnetic elements.

The prepared setup has six led strings, where the number of each string is as follows: $n_{1+} = n_{1-} = 11$, $n_{2+} = n_{2-} = 10$, and $n_{3+} = n_{3-} = 7$. The SRC-based LED driver includes three resonant tanks. Although the experimental setup includes a PIC32 microcontroller (EasyPIC Fusion V7 platform) for ease of use, the proposed driver circuit may be controlled with a simple PWM IC such as SG3525, where the switching frequency may be changed with the help of a potentiometer. An Agilent N2774A DC to 50 MHz current probe is used to monitor the resonant tank current and output current with high resolution.

The results are presented in Figs. 8 and 9. For visual simplicity, only positive channel (Channels 1+, 2+, and 3+) output voltages and currents are presented, since $I_{n+} \cong I_{n-}$ and

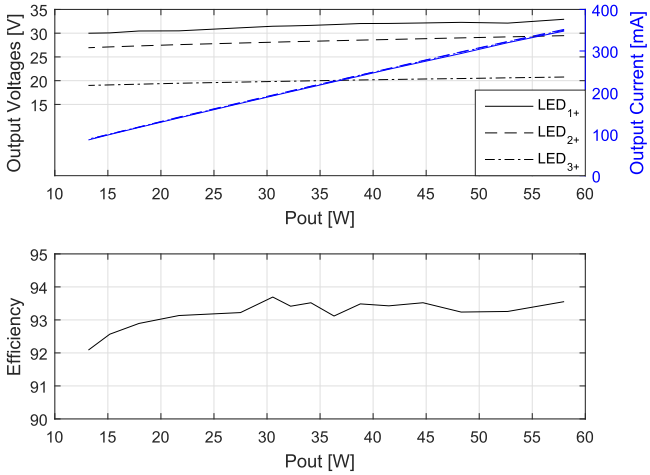

Fig. 9. Illustration of output voltages and currents and efficiency versus output power.

$V_{n+} \cong V_{n-}$. As it can be seen from Fig. 8, the output current increases as the switching frequency is increased. Moreover, the relationship of switching frequency and output current is linear, as predicted.

Additionally, Fig. 8 also includes the illustration of current balancing error. The error is calculated based on the current value of the first LED string. As it can be seen, the error is very small and it is considered to be caused by the differences of resonant capacitors and hand-wound inductances. Fig. 9 illustrates the current and voltage outputs of the channels and the efficiency of the converter. As it can be seen, although output currents of all channels are the same, the output voltages are different. Moreover, it has been verified that the converter operates at high efficiencies for a wide range of output power; although the output power was varied between 13.16 and 58 W by using the dimming feature of the proposed LED driver, the driver efficiency was between 92% and 93.5%.

The resonant tank waveforms of the LED driver are given in Fig. 10(a) to (d), where it is verified that the circuit operates in "k = 2 DCM." The output current and voltage waveforms of the proposed LED driver is illustrated in Fig. 10(e). The rms of current ripple is 11 mA, while the average output current is 350 mA.

Finally, another experimental result is presented, where the following features of the proposed driver are showcased.

1) Capability of providing different current values for each channel: By adjusting the resonant tank values of the associated channel, each channel can be set to provide a different current output value. This enables the construction of very flexible LED driver units for multichannel applications.
2) No-load operation capability: The proposed driver is capable of no-load operation. In this case, the output voltage is equal to V_g.
3) Immunity against cross-regulation among channels: A disturbance or change in one of the channels does not influence the operation of other channels.

For presenting these features, it has been decided to create a scenario, where Channels 1 and 3 are set to provide 350 mA output, whereas Channel 2 is set to provide 700 mA output current for 3-W-rated LEDs, Edison Opto 2ES103BX00000001. This is achieved by adjusting the resonant tank values so that the resonance frequency is maintained to be the same with other channels, while the base impedance is set to be two times smaller than Channels 1 and 3. For this purpose, the resonant tank capacitor is doubled and resonant tank inductance is halved.

In the beginning of the test, all channels are powered, while the voltage outputs of Channels 1 and 3 (350 mA output) and current output of Channel 2 (685 mA output) are being observed. After a while, the LED strings of Channel 3 are disconnected, so that a sudden change in this channel occurs, which in the end causes the output voltage to be equal to $V_g = 100$ V. It can be seen in Fig. 11 that the output voltage of Channel 3 (yellow) suddenly increases, while output voltage of Channel 1 (light blue) and output current of Channel 2 (green) are not affected.

Consequently, the provided experimental results show that the proposed driver circuit exhibits several distinct advantages when compared to the topologies published in the literature.

1) The major advantage of the proposed LED driver is that it inherently ensures a constant output current, within the output voltage boundaries expressed in (21), even when the value of the load changes. Thus, the driver does not require feedback controllers for the purpose of remaining the current at the desired level or ensuring current balancing for each LED string. Consequently, the number of required components for the driver circuit are reduced.
2) The current balancing is ensured, even when the complimentary output stages, V_{n+} and V_{n-} , have different numbers of LEDs.
3) Another distinct feature of this LED driver is that the value of the output current is linearly dependent on the switching frequency so that it operates as a frequency controlled CCS. Thus, the proposed driver presents an inherent dimming capability.
4) Since the control of output current value and current balancing of each LED string are achieved in a single stage, due to inherent features of the SRC, the total number of required components are less, when compared to other studies in the literature. From Table II, it can be seen that all other topologies require either more MOSFETs, diodes or transformers.
5) The results of the experiments show that the proposed circuit operates at reasonably high efficiencies for a very wide output power range. According to the presented results, the driver always operated above 92% efficiency within a range of 14 to 58 W.
6) The proposed LED driver is capable of offering output channels for different current levels.
7) The proposed LED driver is capable of operating at no-load. In no-load operation, the output voltage is equal to V_g.

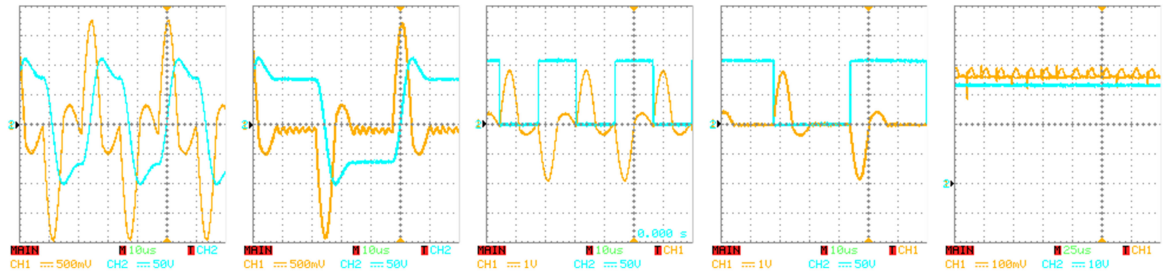

Fig. 10. Waveforms of I_{L_r} (CH1) (1 V/A) and V_{C_r} (CH2) (a) for 350-mA output current (b) for 175-mA output current. Waveforms of I_{L_r} (CH1) (1 V/A) and V_{ds1} (CH2) (c) for 350-mA output current (d) for 175-mA output current. (e) Output current and voltage waveforms.

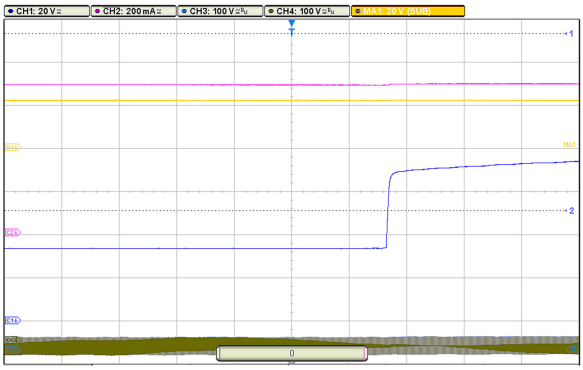

Fig. 11. Results of the experiment, where CH1 (blue) is the output voltage of Channel 3, CH2 (purple) is the output current of channel 2 and MA1 (yellow) is the output voltage of Channel 1.

VI. Conclusion

In this study, the literature on multichannel LED drivers is reviewed and a multichannel LED driver based on the SRC is proposed. The proposed driver circuit utilized the fact that the SRC operates as a frequency controlled current source in "k = 2 DCM" operation mode, where the relationship of frequency and output current is linear.

It has been experimentally shown that the proposed driver exhibited distinct advantages by being able to provide good current accuracy and current sharing among different LED strings, while ensuring these features in a single stage and even in open-loop operation. Moreover, efficiency values competitive with the literature has been achieved, while exhibiting relative advantages either in control simplicity or circuit complexity or in both.

On the other hand, the major disadvantage of the proposed driver is that the output voltage of the driver circuit is limited to a specific range, as shown in (10) and (21). Thus, the minimum and maximum numbers of LEDs in a string are limited. However, this range can be altered by utilization of transformers, if needed. Additionally, the output current value is dependent on the resonant tank elements. As observed in the experiment, different values of resonant inductors and capacitors cause slight current balancing errors. However, it is shown that the values of the errors are very low, although the inductors were hand-wound. It is predicted that utilization of planar inductance technology would further minimize these errors.

References

[1] S. Winder, *Power Supplies for LED Drivers*. Burlington, MA, USA: Newnes, 2008.
[2] D. Shmilovitz, A. Abramovitz, and I. Reichman, "Quasi-resonant led driver with capacitive isolation and high pf," *IEEE J. Emerg. Sel. Topics Power Electron.*, vol. 3, no. 3, pp. 633–641, Sep. 2015.
[3] Y. Hu and M. M. Jovanovic, "Led driver with self-adaptive drive voltage," *IEEE Trans. Power Electron.*, vol. 23, no. 6, pp. 3116–3125, Nov. 2008.
[4] A. Zhao and W. T. Ng, "An energy conservation based high-efficiency dimmable multi-channel led driver," in *Proc. IEEE Energy Convers. Congr. Expo.*, Sep. 2011, pp. 2576–2580.
[5] H. C. Kim, C. S. Yoon, H. Ju, D. K. Jeong, and J. Kim, "An ac-powered, flicker-free, multi-channel led driver with current-balancing simo buck topology for large area lighting applications," in *Proc. IEEE Appl. Power Electron. Conf. Expo.*, Mar. 2014, pp. 3337–3341.
[6] T. Jeong and J. Kim, "A 110-v ac, 17.1-w multi-segmented led driver with 96.2 power factor," in *Proc. IEEE Appl. Power Electron. Conf. Expo.*, Mar. 2015, pp. 896–899.
[7] H. C. Kim, C. S. Yoon, D. K. Jeong, and J. Kim, "A single-inductor, multiple-channel current-balancing led driver for display backlight applications," *IEEE Trans. Ind. Appl.*, vol. 50, no. 6, pp. 4077–4081, Nov. 2014.
[8] R. Wang and J. Zhang, "A simple current balancing method for multi-output flyback led driver," in *Proc. IEEE 2nd Int. Future Energy Electron. Conf.*, Nov. 2015, pp. 1–5.
[9] W. Chen and S. Y. R. Hui, "A dimmable light-emitting diode (led) driver with mag-amp postregulators for multistring applications," *IEEE Trans. Power Electron.*, vol. 26, no. 6, pp. 1714–1722, Jun. 2011.
[10] K. Modepalli and L. Parsa, "A scalable n-color led driver using single inductor multiple current output topology," *IEEE Trans. Power Electron.*, vol. 31, no. 5, pp. 3773–3783, May 2016.
[11] Y. Guo, S. Li, A. T. L. Lee, S. C. Tan, C. K. Lee, and S. Y. R. Hui, "AC-DC single-inductor multiple-output led drivers," Chinese Patent PCT/CN2015/077 290, Oct. 27, 2016.
[12] Y. Guo, S. Li, A. T. L. Lee, S. C. Tan, C. K. Lee, and S. Y. R. Hui, "Single-stage ac/dc single-inductor multiple-output led drivers," *IEEE Trans. Power Electron.*, vol. 31, no. 8, pp. 5837–5850, Aug. 2016.
[13] H. Chen, Y. Zhang, and D. Ma, "A simo parallel-string driver ic for dimmable led backlighting with local bus voltage optimization and single time-shared regulation loop," *IEEE Trans. Power Electron.*, vol. 27, no. 1, pp. 452–462, Jan. 2012.
[14] A. T. L. Lee, J. K. O. Sin, and P. C. H. Chan, "Scalability of quasi-hysteretic fsm-based digitally controlled single-inductor dual-string buck led driver to multiple strings," *IEEE Trans. Power Electron.*, vol. 29, no. 1, pp. 501–513, Jan. 2014.
[15] Q. Luo, S. Zhi, C. Zou, W. Lu, and L. Zhou, "An led driver with dynamic high-frequency sinusoidal bus voltage regulation for multistring applications," *IEEE Trans. Power Electron.*, vol. 29, no. 1, pp. 491–500, Jan. 2014.
[16] Q. Luo, K. Ma, Q. He, C. Zou, and L. Zhou, "A single stage high frequency resonant ac/ac converter," *IEEE Trans. Power Electron.*, vol. 32, no. 3, pp. 2155–2166, Mar. 2017.
[17] X. Chen, D. Huang, Q. Li, and F. Lee, "Multichannel led driver with CLL resonant converter," *IEEE J. Emerg. Sel. Topics Power Electron.*, vol. 3, no. 3, pp. 589–598, Sep. 2015.
[18] J. Zhang, J. Wang, and X. Wu, "A capacitor-isolated led driver with inherent current balance capability," *IEEE Trans. Ind. Electron.*, vol. 59, no. 4, pp. 1708–1716, Apr. 2012.

[19] T. Jiang, J. Wang, J. Zhang, and X. Wu, "Hybrid passive current sharing method for multi-channel SRC led driver," in *Proc. IEEE Energy Convers. Congr. Expo.*, Sep. 2013, pp. 4646–4649.
[20] X. Wu, C. Hu, J. Zhang, and Z. Qian, "Analysis and design considerations of LLCC resonant multioutput DC/DC led driver with charge balancing and exchanging of secondary series resonant capacitors," *IEEE Trans. Power Electron.*, vol. 30, no. 2, pp. 780–789, Feb. 2015.
[21] R. Zhao and J. Zhang, "High efficiency hybrid current balancing method for multi-channel led drive," in *Proc. IEEE Appl. Power Electron. Conf. Expo.*, Mar. 2015, pp. 854–860.
[22] X. Qu, S. C. Wong, and C. K. Tse, "An improved LCLC current-source-output multistring led driver with capacitive current balancing," *IEEE Trans. Power Electron.*, vol. 30, no. 10, pp. 5783–5791, Oct. 2015.
[23] H. Ma, J. S. Lai, C. Zheng, and P. Sun, "A high-efficiency quasi-single-stage bridgeless electrolytic capacitor-free high-power ac-dc driver for supplying multiple led strings in parallel," *IEEE Trans. Power Electron.*, vol. 31, no. 8, pp. 5825–5836, Aug. 2016.
[24] S. H. Cho, S. H. Lee, S. S. Hong, D. S. Oh, and S. K. Han, "High-accuracy and cost-effective current-balanced multichannel led backlight driver using single-transformer," in *Proc. IEEE 8th Int. Conf. Power Electron. ECCE Asia*, May 2011, pp. 520–527.
[25] S. S. Hwang, W. S. Hwang, B. J. Jang, S. K. Han, and J. I. Kang, "Cost-effective single switch multi-channel led driver," in *Proc. 16th Int. Power Electron. Motion Control Conf. Expo.*, Sep. 2014, pp. 156–161.
[26] K. Afridi, "The series resonant converter," [Online]. Available: http://ecee.colorado.edu/ ecen5817/notes/ch4.pdf
[27] B. Yang, "Topology investigation of front end dc/dc converter for distributed power system," Ph.D. dissertation, Virginia Polytech. Inst. State Univ., Blacksburg, VA, USA, Sep. 2003. [Online]. Available: https://vtechworks.lib.vt.edu/handle/10919/28982

Taha Nurettin Gücin received the B.Sc. degree from Istanbul Technical University (ITU), Istanbul, Turkey, in 2010. He received the M.Sc. degree from Energy Institute, ITU, in 2013. He is currently working toward the Ph.D. degree at Electrical Engineering Department, ITU.

He is a Power Supply Engineer with Elettra Sincrotrone Trieste, Basovizza, Italy. His research interests include power electronics, electrical machines and drives, and renewable energy systems.

Bekir Fincan received the B.Sc. degree from Istanbul Technical University (ITU), in 2012. He received the M.Sc. degree from Electrical Engineering Department, ITU, in 2015. He is currently working toward the Ph.D. degree with Electrical Engineering Department, ITU.

He is a Power Electronics Engineer with Pavotek Electronics, Istanbul, Turkey. He has been engaged in research and development of wireless charging for electrical vehicles and drivers for BLDC hub motors in order to use electrical vehicles. His research interests include wireless energy transfer, power electronics, electrical vehicles, and electrical machines and drives.

Muhammet Biberoğlu received the B.Sc. degree from Eskişehir Osmangazi University, Eskişehir, Turkey, in 2010. He received the M.Sc. degree from Istanbul Technical University (ITU), in 2013. He has been working toward the Ph.D. degree with Electrical Engineering Department, ITU, since 2013.

He is a Research Assistant with the Energy Systems Engineering Department, University of Yalova, Yalova, Turkey. His research interests include renewable energy technologies, power electronics, electric machines, and control systems.